

External forward shock origin of high energy emission for three GRBs detected by *Fermi*

P. Kumar^{1*} and R. Barniol Duran^{1,2*}

¹*Department of Astronomy, University of Texas at Austin, Austin, TX 78712, USA*

²*Department of Physics, University of Texas at Austin, Austin, TX 78712, USA*

Accepted 2010 June 30; Received 2010 June 29; in original form 2009 October 27

ABSTRACT

We analyze the >100 MeV data for 3 GRBs detected by the *Fermi* satellite (GRBs 080916C, 090510, 090902B) and find that these photons were generated via synchrotron emission in the external forward shock. We arrive at this conclusion by four different methods as follows. (1) We check the light curve and spectral behavior of the >100 MeV data, and late time X-ray and optical data, and find them consistent with the so called closure relations for the external forward shock radiation. (2) We calculate the expected external forward shock synchrotron flux at 100 MeV, which is essentially a function of the total energy in the burst alone, and it matches the observed flux value. (3) We determine the external forward shock model parameters using the >100 MeV data (a very large phase space of parameters is allowed by the high energy data alone), and for each point in the allowed parameter space we calculate the expected X-ray and optical fluxes at late times (hours to days after the burst) and find these to be in good agreement with the observed data for the entire parameter space allowed by the >100 MeV data. (4) We calculate the external forward shock model parameters using only the late time X-ray, optical and radio data and from these estimate the expected flux at >100 MeV at the end of the sub-MeV burst (and at subsequent times) and find that to be entirely consistent with the high energy data obtained by *Fermi*/LAT. The ability of a simple external forward shock, with two empirical parameters (total burst energy and energy in electrons) and two free parameters (circum-stellar density and energy in magnetic fields), to fit the entire data from the end of the burst (1–50s) to about a week, covering more than eight-decades in photon frequency — $>10^2$ MeV, X-ray, optical and radio — provides compelling confirmation of the external forward shock synchrotron origin of the >100 MeV radiation from these *Fermi* GRBs. Moreover, the parameters determined in points (3) and (4) show that the magnetic field required in these GRBs is consistent with shock-compressed magnetic field in the circum-stellar medium with pre-shocked values of a few tens of micro-Gauss.

Key words: radiation mechanisms: non-thermal - methods: numerical, analytical - gamma-ray burst: individual: 080916C, 090510, 090902B.

1 INTRODUCTION

The *Fermi* Satellite has opened a new and sensitive window in the study of GRBs (gamma-ray bursts); for a general review of GRBs see Gehrels, Ramirez-Ruiz & Fox (2009), Mészáros (2006), Piran (2004), Woosley & Bloom (2006), Zhang (2007). So far, in about one year of operation, *Fermi* has detected 12 GRBs with photons with energies >100 MeV. The $>10^2$ MeV emission of most bursts detected by the LAT (Large Area Telescope: energy coverage 20 MeV to >300 GeV) instrument aboard the *Fermi* satellite shows two very interesting features (Omedei et al. 2009): (1) The first >100 MeV photon arrives later than the first lower energy photon

($\lesssim 1$ MeV) detected by GBM (Gamma-ray Burst Monitor), (2) The >100 MeV emission lasts for much longer time compared to the burst duration in the sub-MeV band (the light curve in sub-MeV band declines very rapidly).

There are many possible >100 MeV photons generation mechanisms proposed in the context of GRBs; see Gupta & Zhang (2007) and Fan & Piran (2008) for a review. Shortly after the observations of GRB 080916C (Abdo et al. 2009a), we proposed a simple idea: the >100 MeV photons in GRB 080916C are produced via synchrotron emission in the external forward shock (Kumar & Barniol Duran 2009). This proposal naturally explains the observed delay in the peak of the light curve for >100 MeV photons – it corresponds to the deceleration time-scale of the relativistic ejecta – and also the long lasting >100 MeV emission, which

* E-mail: pk@astro.as.utexas.edu, rbarniol@physics.utexas.edu

	β_{LAT}	p	z	d_{L28}	$t_{GRB}[s]$	$E_{\gamma,iso}[erg]$
GRB 080916C	1.20 ± 0.03	2.4 ± 0.06	4.3	12.3	60	8.8×10^{54}
GRB 090510	1.1 ± 0.1	2.2 ± 0.2	0.9	1.8	0.3	1.08×10^{53}
GRB 090902B	1.1 ± 0.1	2.2 ± 0.2	1.8	4.3	30	3.63×10^{54}

Table 1. The main quantities used in our analysis for these 3 GRBs. β_{LAT} is the spectral index for the > 100 MeV data, p is the power-law index for the energy distribution of injected electrons i.e. $dn/d\gamma \propto \gamma^{-p}$, z is the redshift, d_{L28} is the luminosity distance in units of 10^{28} cm, t_{GRB} is the approximate burst duration in the *Fermi*/GBM band and $E_{\gamma,iso}$ is the isotropic equivalent of energy observed in γ -rays in the 10keV-10GeV band for GRB080916C and GRB090902B, and in the 10keV-30GeV band for GRB090510. Data taken from Abdo et al. (2009a, 2009b, 2009c), De Pasquale et al. (2010).

corresponds to the power-law decay nature of the external forward shock (ES) emission (the ES model was first proposed by Rees & Mészáros 1992, Mészáros & Rees 1993, Paczyński & Rhoads 1993; for a comprehensive review of the ES model, see, e.g., Piran, 2004, and references therein). Following our initial analysis on GRB 080916C, a number of groups have provided evidence for the external forward shock origin of *Fermi*/LAT observations (Gao et al. 2009; Ghirlanda, Ghisellini, Nava 2010; Ghisellini, Ghirlanda, Nava 2010; De Pasquale et al. 2010).

In this paper we analyze the >100 MeV emission of GRB 090510 and GRB 090902B in detail, and discuss the main results of our prior calculation for GRB 080916C (Kumar & Barniol Duran 2009), to show that the high energy radiation for all these three arose in the external forward shock via the synchrotron process. These three bursts - one short and two long GRBs - are selected in this work because the high energy data for these bursts have been published by the *Fermi* team as well as the fact that they have good afterglow follow up observations in the X-ray and optical bands (and also the radio band for GRB 090902B) to allow for a thorough analysis of data covering more than a factor 10^8 in frequency and $> 10^4$ in time to piece together the high energy photon generation mechanism, and cross check this in multiple different ways.

In the next section (§2) we provide a simple analysis of the LAT spectrum and light curve for these three bursts to show that the data are consistent with the external forward shock model. This analysis consists of verifying whether the temporal decay index and the spectral index satisfy the relation expected for the ES emission (closure relation), and comparing the observed flux in the LAT band with the prediction of the ES model (according to this model the high energy flux is a function of blast wave energy, independent of the unknown circum-stellar medium density, and extremely weakly dependent on the energy fraction in magnetic fields).

We describe in §3 how the >100 MeV data alone can be used to theoretically estimate the emission at late times ($t \gtrsim$ a few hours) in the X-ray and optical bands within the framework of the external forward shock model, and that for these three bursts the expected flux according to the ES model is in agreement with the observed data in these bands.

Moreover, if we determine the ES parameters (ϵ_e , ϵ_B , n , and E)¹ using only the late time X-ray and optical fluxes (and radio data), we can predict the flux at >100 MeV at any time after the deceleration time for the GRB relativistic outflow. We show in §3 that this predicted flux at $> 10^2$ MeV is consistent with the value observed by the *Fermi* satellite for the bursts analyzed in this paper.

These exercises and results show that the high energy emission

is due to the external shock as discussed in §3. We also describe in §3 that the magnetic field in the shocked fluid — responsible for the generation of > 100 MeV photons as well as the late time X-ray and optical photons via the synchrotron mechanism — is consistent with the shock compression of a circum-stellar magnetic field of a few tens of micro-Gauss.

It is important to point out that we do not consider in this work the prompt sub-MeV emission mechanism for GRBs — which is well known to have a separate and distinct origin as evidenced by the very rapid decay of sub-MeV flux observed by Swift and *Fermi*/GBM (the flux in the sub-MeV band drops-off with time as $\sim t^{-3}$ or faster as opposed to the $\sim t^{-1}$ observed in the LAT band). Nor do we investigate the emission process for photons in the LAT band during the prompt burst phase.

2 ES MODEL AND THE >100 MEV EMISSION FROM GRBS: SIMPLE ARGUMENTS

In this work we consider 3 GRBs detected by *Fermi*/LAT in the $> 10^2$ MeV band: GRB 080916C (Abdo et al. 2009a), GRB 090510 (Abdo et al. 2009b, De Pasquale et al. 2010) and GRB 090902B (Abdo et al. 2009c). These bursts show the “generic” features observed in the >100 MeV emission of most of *Fermi* GRBs mentioned above, and these are the only three bursts for which we have optical, X-ray and *Fermi* data available. Some basic information for these 3 GRBs have been summarized in Table 1.

The synchrotron process in the ES model predicts a relationship between the temporal decay index (α) of the light curve and the energy spectral index (β), which are so called closure relations. These relations serve as a quick check for whether or not the observed radiation is being produced in the external shock. In this paper, we use the convention $f(\nu, t) \propto \nu^{-\beta} t^{-\alpha}$.

Since the *Fermi*/LAT band detects very high energy photons ($\gtrsim 10^2$ MeV), it is reasonable to assume that this band lies above all the synchrotron characteristic frequencies (assuming that the emission process is synchrotron). In this case the spectrum should be $\propto \nu^{-p/2}$ (Sari, Piran, Narayan 1998)— where p is the power law index of the injected electrons’ energy distribution — and according to the external forward shock model (see, e.g., Panaitescu & Kumar 2000), the light curve should decay as $\propto t^{-(3p-2)/4}$, giving the following closure relation: $\alpha = (3\beta - 1)/2$. Using the data in Table 1 we find that all three bursts satisfy this closure relation (Table 2), which encourages us to continue our diagnosis of the >100 MeV emission in the context of the ES model.

We next check to see if the predicted magnitude of the synchrotron flux in the ES is consistent with the observed values. This calculation would seem very uncertain at first, but we note that the predicted external forward shock synchrotron flux at a frequency larger than all characteristic frequencies of the synchrotron emis-

¹ ϵ_e and ϵ_B are the energy fraction in electrons and magnetic field for the shocked fluid, n is the number density of protons in the burst circum-stellar medium, and E is the kinetic energy in the ES blast wave.

	α_{ES}	α_{obs}	$t[s]$	$f_{100MeV}^{ES}{}^a$	f_{100MeV}^{obs}
GRB 080916C	1.30 ± 0.05	1.2 ± 0.2	150	> 16	67
GRB 090510	1.2 ± 0.2	1.38 ± 0.07	100	> 3	14
GRB 090902B	1.2 ± 0.2	~ 1.5	50	> 100	220

^a Fluxes in this table are in nJy . The fluxes are calculated using equation (1), the data in Table 1, and setting the isotropic kinetic energy in the ES to be $E = E_{\gamma,iso}$, which gives a lower limit on E ; most likely $E = \text{few} \times E_{\gamma,iso}$ and we find that using $E \sim 3 \times E_{\gamma,iso}$ the fluxes match the observed values very well. Also, for this calculation, $\epsilon_B = 10^{-5}$, $\epsilon_e = 0.25$, $p = 2.4$ and $Y < 1$.

Table 2. Comparison between the temporal decay index (α_{ES}) expected for the external forward shock model, and the observed decay index (α_{obs}); these values are equal to within $1-\sigma$ error bar. The ES flux calculated at time t is compared to the observed value at the same time. These two values are also consistent, further lending support to the ES origin of the > 100 MeV emission. Data are obtained from the same references as in Table 1. The theoretically calculated flux would be larger if $\epsilon_e > 0.25$; GRB afterglow data for 8 well studied bursts suggest that $0.2 < \epsilon_e \lesssim 0.8$ (Panaitescu & Kumar 2001).

sion is independent of the circum-stellar medium (CSM) density, n , and it is extremely weakly dependent on the fraction of the energy of the shocked gas in the magnetic field, ϵ_B , which is a highly uncertain parameter for the ES model. The density falls off as $\propto R^{-s}$, where R is the distance from the center of the explosion, and $s = 0$ corresponds to a constant CSM and $s = 2$ corresponds to a CSM carved out by the progenitor star’s wind. The flux is given by (see e.g. Kumar 2000, Panaitescu & Kumar 2000):

$$f_\nu = 0.2mJy E_{55}^{\frac{p+2}{4}} \epsilon_e^{p-1} \epsilon_{B,-2}^{\frac{p-2}{4}} t_1^{-\frac{3p-2}{4}} \nu_8^{-\frac{p}{2}} (1+Y)^{-1} \times (1+z)^{\frac{p+2}{4}} d_{L28}^{-2}, \quad (1)$$

where ϵ_e is the fraction of energy of the shocked gas in electrons, $t_1 = t/10s$ is the time since the beginning of the explosion in the observer frame (in units of 10s), ν_8 is photon energy in units of 100MeV, $E_{55} = E/10^{55}$ erg is the scaled isotropic kinetic energy in the ES, Y is the Compton- Y parameter, z is the redshift and d_{L28} is the luminosity distance to the burst (in units of 10^{28} cm). Using the values of Table 1, we can predict the expected flux at 100 MeV from the ES and compare it to the observed value at the same time. We show in Table 2 that the observed high energy flux is consistent with the theoretically expected values for all three bursts.

The fact that these bursts satisfy the closure relation, and that the observed $> 10^2$ MeV flux is consistent with theoretical expectations, suggests that the high energy emission detected by *Fermi*/LAT from GRBs is produced via synchrotron emission in the ES. In the next section we carry out a more detailed analysis that includes all the available data from these bursts during the “afterglow” phase, i.e. after the emission in the sub-MeV band has ended (or fallen below *Fermi*/GBM threshold).

3 DETAILED SYNTHESIS OF ALL AVAILABLE DATA AND THE EXTERNAL FORWARD SHOCK MODEL

The simple arguments presented in the last section provide tantalizing evidence that the high energy photons from the three bursts considered in this paper are synchrotron photons produced in the external forward shock. We present a more detailed analysis in this section where we consider all available data for the three bursts after the end of the emission in the *Fermi*/GBM band, i.e. for $t > t_{GRB}$, where t_{GRB} is the “burst duration” provided in Table 1. The data we consider consist of $> 10^2$ MeV emission observed by *Fermi*/LAT and AGILE/GRID, X-ray data from Swift/XRT, optical data from Swift/UVOT and various ground based observatories, and radio data from Westerbork in the case of GRB 090902B.

The *main idea* is to use the $> 10^2$ MeV data to constrain the ES parameters (ϵ_e , ϵ_B , n and E)² — which as we shall see allow for a large hyper-surface in this space — and for each of the points in the allowed 4-D parameter space calculate the flux in the X-ray, optical and radio bands from the external forward shock at those times where data in one of these bands are available for comparison with the observed value. It would be tempting to think that such an exercise cannot be very illuminating as the ES flux calculated at any given time in these bands would have a large uncertainty that would reflect the large volume of the sub-space of 4-D parameter space allowed by the $> 10^2$ MeV data alone. This, however, turns out to be incorrect — the afterglow flux generated by the ES in the X-ray and optical bands (before the time of jet break) is almost uniquely determined from the high-energy photon flux; the entire sub-space of the 4-D space, allowed by the $> 10^2$ MeV data, projects to an extremely small region (almost to a point) as far as the emission at any frequency larger than $\sim \nu_i$ is concerned; ν_i is the synchrotron frequency corresponding to the minimum energy of injected electrons (electrons just behind the shock front), which we also refer to as synchrotron injection frequency. Therefore, we can compare the ES model predictions of flux in the X-ray and optical bands with the observed data, and either rule out the ES origin for high energy photons or confirm it³.

We also carry out this exercise in the *reverse direction*, i.e. find the sub-space of 4-D parameter space allowed by the late time ($t \gtrsim 1$ day) X-ray, optical, and radio data, and then calculate the expected $> 10^2$ MeV flux at early times for this allowed subspace for comparison with the observed *Fermi*/LAT data. This *reverse direction* exercise is not equivalent to the one described in the preceding paragraph since the 4-D sub-space allowed by the $> 10^2$ MeV data and that by the late time X-ray and optical data are in general quite different (of course they have common points whenever early high-energy and late low energy emissions arise from the same ES).

The input physics in all of these calculations consist of the following main ingredients: synchrotron frequency and flux (see Rybicki & Lightman 1979 for detailed formulae; a convenient sum-

² In addition to these four parameters, the ES model also has an extra two, which are s and p . However, these last two can be estimated fairly directly by looking at the spectrum and temporal decay indexes of the light curves at different wavelengths.

³ It should be pointed out that the X-ray afterglow light curves of long-GRBs are rather complicated during the first few hours (see e.g. Nousek et al. 2006, O’Brien et al. 2006) and the ES model in its simplest form can’t explain these features, however the behavior becomes simpler and consistent with ES origin after about 1/2 day.

mary of the relevant equations can also be found in Kumar & Narayan (2009), Blandford-McKee self-similar solution for the ES (Blandford & McKee 1976), electron cooling due to synchrotron and synchrotron self-Compton radiation (Klein-Nishina reduction to the cross-section is very important to incorporate for all the three bursts for at least a fraction of the 4-D parameter space), and the emergent synchrotron spectrum as described in e.g. Sari, Piran & Narayan (1998). Although the calculations we present in the following sections can be carried out analytically (e.g. Kumar & McMahan 2008), it is somewhat tedious, and so we have coded all the relevant physics in a program and use that for finding the allowed part of 4-D parameter space and for comparing the results of theoretical calculation with the observed data. Numerical codes have also the advantage that they enable us to make fewer assumptions and approximations. Nevertheless, we present a few analytical estimates to help the reader a flavor of the calculations involved.

We analyze the data for each of the three bursts individually in the following three sub-sections in reverse chronological order.

3.1 GRB 090902B

The *Fermi*/LAT and GBM observations of this burst can be found in Abdo et al. (2009c). The X-ray data for this GRB started at about half a day after the trigger time. The spectrum in the 0.3–10 keV X-ray band was found to be $\beta_x = 0.9 \pm 0.1$, and the light curve decayed as $\alpha_x = 1.30 \pm 0.04$ (Pandey et al. 2010). The optical observations by Swift/UVOT started at the same time (Swenson & Stratta 2009) and show $\alpha_{opt} \sim 1.2$. ROTSE also detected the optical afterglow starting at ~ 1.4 hours and its decay is consistent with the UVOT decay (Pandey et al. 2009). The Faulkes Telescope North also observed the afterglow at about 21 hours after the burst using the R filter (Guidorzi et al. 2009). There is a radio detection available at about 1.3 days after the burst and its flux is $\sim 111 \mu\text{Jy}$ at 4.8GHz (van der Host et al. 2009).

The late time afterglow data obtained by Swift/XRT show that the X-ray band, 0.3–10 keV (ν_x), should lie between ν_i (the synchrotron injection frequency) and ν_c (the synchrotron frequency corresponding to the electrons' energy for which the radiative loss time-scale equals the dynamical time; we also refer to it as synchrotron cooling frequency). This is because $\nu_x > \nu_i$, otherwise the light curve would be rising with time instead of the observed decline. Moreover, if $\nu_c < \nu_x$, then $p = 2\beta_x \sim 1.8 \pm 0.2$, and in that case $f_{\nu_x}(t) \propto t^{-(3p+10)/16} = t^{-0.96 \pm 0.04}$, and that is inconsistent with the observed decline of the X-ray light curve (for decay indices for values of $p < 2$ see the table 1 in Zhang & Mészáros (2004)). Thus, $\nu_i < \nu_x < \nu_c$, so that $\beta_x = (p - 1)/2$ or $p \sim 2.8 \pm 0.2$.

Next we determine if the X-ray data are consistent with a constant density circum-stellar medium or a wind-like medium. For $s = 0$ ($s = 2$) the expected temporal decay index of the X-ray light curve is $\alpha = 3(p - 1)/4 = 1.35 \pm 0.15$ ($\alpha = (3p - 1)/4 = 1.85 \pm 0.15$). Thus, a constant density circum-stellar medium is favored for this GRB.

The XRT flux at 1keV at $t = 12.5\text{hr}$ was reported to be $0.4 \mu\text{Jy}$ (Pandey et al. 2010). Extrapolating this flux to the optical band using the observed values of α_x and β_x we find the flux at 21hr to be within a factor ~ 3 of the $\sim 15 \mu\text{Jy}$ flux reported by Guidorzi et al. (2009). Thus, the emissions in the optical and the X-ray bands arise in the same source (ES) with ν_i below the optical band; also, if the optical band were below ν_i , then the optical light curve would be increasing with time, which is not observed. Moreover, the optical and X-ray data together provide a more accurate determination of

the spectral index to be 0.69 ± 0.06 or $p = 2.38 \pm 0.12$ which is consistent with the p -value for the high-energy data at $t > t_{GRB}$ (see Table 1).

If the $>10^2\text{MeV}$ emission is produced in the external forward shock then we should be able to show that the early high energy γ -ray flux is consistent with the late time X-ray and optical data. We first show this approximately using analytical calculations, and then present results obtained by a more accurate numerical calculation in our figures.

The observed flux at 100 MeV and $t = 50\text{s}$ can be extrapolated to half a day to estimate the flux at 1 keV. This requires the knowledge of where ν_c lies at this time. It can be shown that $\nu_c \sim 100\text{MeV}$ at 50 s in order that the flux at 100 keV does not exceed the observed flux limit (see subsection below). Therefore, $\nu_c \propto t^{-1/2}$ is $\sim 3\text{MeV}$ at 12.5 hr, and thus the expected flux at 1 keV is $\sim 0.5 \mu\text{Jy}$ which agrees with the observed value. Therefore, we can conclude that the $>100\text{MeV}$, X-ray and optical photons were all produced by the same source, and we suggest that this source must be the external forward shock as already determined for the X-ray and optical data.

We now turn to determining the ES parameter space for this burst. We can determine this space using both the forward direction and reverse direction approaches. We first list the constraints on the ES model, then give a few analytical estimates using the equations in, for example, Panaitescu & Kumar (2002), and then present the results of our detail numerical calculations.

3.1.1 Forward direction

In this subsection we only use the early high-energy emission to constrain the ES parameter space. The constraints at $t = 50\text{s}$ are: (i) The flux at 100 MeV should agree with the observed value (see Table 2) - within the error bar of 10%, (ii) $\nu_c < 100\text{MeV}$ at 50s for consistency with the observed spectrum, (iii) the flux at 100 keV should be smaller than 0.04 mJy (which is a factor of 10 less than the observed value), so that ES emission does not prevent the *Fermi*/GBM light curve to decay steeply after 25 seconds, and (iv) $Y < 50$ so that the energy going into the second Inverse Compton is not excessive.

The first 3 conditions give the following 3 equations at $t = 50\text{s}$. The cooling frequency is given by (Panaitescu & Kumar 2002)

$$\nu_c \sim 6\text{eV} E_{55}^{-1/2} n^{-1} \epsilon_{B,-2}^{-3/2} (1 + Y)^{-2} < 100\text{MeV}. \quad (2)$$

The flux at 100 keV, which is between ν_i and ν_c as discussed above, is (Panaitescu & Kumar 2002)

$$f_{100\text{keV}} \sim 53\text{mJy} E_{55}^{1.35} n^{0.5} \epsilon_{B,-2}^{0.85} \epsilon_{e,-1}^{1.4} < 0.04\text{mJy}. \quad (3)$$

And lastly, using (1), the flux at 100 MeV, which we assume is above ν_c , is

$$f_{100\text{MeV}} \sim 1 \times 10^{-4} \text{mJy} E_{55}^{1.1} \epsilon_{B,-2}^{0.1} \epsilon_{e,-1}^{1.4} = 220\text{nJy}. \quad (4)$$

Solving for n from (3) and for ϵ_e from (4), and substituting in (2), we find that at 50 s $\nu_c \gtrsim 50\text{MeV}$. The injection frequency can also be estimated at $t = 50\text{s}$, it is given by

$$\nu_i \sim 8\text{keV} E_{55}^{1/2} \epsilon_{B,-2}^{1/2} \epsilon_{e,-1}^2, \quad (5)$$

and using (4), one finds $\nu_i \sim 25\text{keV} E_{55}^{-1.07} \epsilon_{B,-2}^{0.36}$, which gives $\nu_i \sim 2\text{keV}$ for $\epsilon_B \sim 10^{-5}$. These values of ν_i and ν_c are consistent with the values obtained with detail numerical calculations and reported in the Fig. 1 caption.

Using (2), we can find a lower limit on ϵ_B , which is given by

$$\epsilon_B \gtrsim \frac{1 \times 10^{-7}}{n^{2/3} E_{55}^{1/3} (1+Y)^{4/3}}. \quad (6)$$

Also, we can solve for ϵ_e using (4) and substitute that into (3) to obtain an upper limit on ϵ_B , which is

$$\epsilon_B \lesssim \frac{3 \times 10^{-7}}{n^{2/3} E_{55}^{1/3} (1+Y)^{4/3}}. \quad (7)$$

Note that these estimates are consistent with the numerical results we present in Fig. 1. We also find the $\epsilon_B \propto n^{-2/3}$ dependence that is shown in the figure.

Moreover, with these parameters we can predict the fluxes at late times. The X-ray and optical band lie between ν_i and ν_c at ~ 1 day (see above). The first X-ray data point is at 12.5 hr, and the theoretically expected flux at 1 keV at this time is given by

$$f_{1\text{keV}} \sim 1\text{mJy} E_{55}^{1.35} n^{0.5} \epsilon_{B,-2}^{0.85} \epsilon_{e,-1}^{1.4}, \quad (8)$$

and the optical flux at $\sim 7.5 \times 10^4$ s is

$$f_{2eV} \sim 47\text{mJy} E_{55}^{1.35} n^{0.5} \epsilon_{B,-2}^{0.85} \epsilon_{e,-1}^{1.4}. \quad (9)$$

We can use (3) to find an upper limit for the X-ray and optical fluxes. In addition, we can find ϵ_e using (4), and use (6) to find a lower limit for these fluxes. We find that

$$0.5\mu\text{Jy} \lesssim f_{1\text{keV}} \lesssim 0.8\mu\text{Jy} \quad (10)$$

for the X-ray flux at 12.5 hr, and

$$25\mu\text{Jy} \lesssim f_{2eV} \lesssim 36\mu\text{Jy} \quad (11)$$

for the optical flux at $\sim 7.5 \times 10^4$ s. These estimates agree very well with the observed values of $0.4\mu\text{Jy}$ (Pandey et al. 2010) and $15\mu\text{Jy}$ (Guidorzi et al. 2009) at the respective bands and times. We note that, although Inverse Compton cooling is very important at late times, the X-ray band lies below ν_c and therefore X-ray and optical fluxes are unaffected by Inverse Compton cooling.

Next, we present the results obtained by detailed numerical calculations. We use the same constraints described at the beginning of this subsection to determine the parameter space allowed by the high-energy early data. It is worth noting that in our numerical calculations throughout the paper we make no assumption regarding the ordering of the characteristic frequencies, nor the location of the observed bands with respect to them. The projection of the sub-space of the 4-D parameter space allowed by the high energy data onto the ϵ_B - n plane is shown in Figure 1, and some of the other ES parameters are presented in the Fig. 1 caption. It is clear that there is a large sub-space that is consistent with the LAT data, and also that the magnetic field needed for the synchrotron source is consistent with the shock-compressed magnetic field in the CSM of strength $\lesssim 30\mu\text{G}$. For each point in the 4-D space allowed by the $>10^2\text{MeV}$ data we calculate the X-ray and the optical flux at late times. In spite of the fact that the 4-D sub-space allowed by the LAT data is very large (fig. 1) the expected X-ray and optical flux at late times lie in a narrow range as shown by two diagonal bands in Figure 2; the width of these bands has been artificially increased by a factor 2 to reflect the approximate treatment of the radial structure of the blast wave and also to include in the calculation the effect of the blast wave spherical curvature on the ES emission (see, e.g., Appendix A of Panaitescu & Kumar 2000; both of these effects together contribute roughly a factor of 2). We see that the observed X-ray and optical light curves lie within the theoretically calculated bands (Fig. 2). This result strongly supports the ES model for the origin of the $>10^2\text{MeV}$ photons.

We note that the above mentioned extrapolation from early

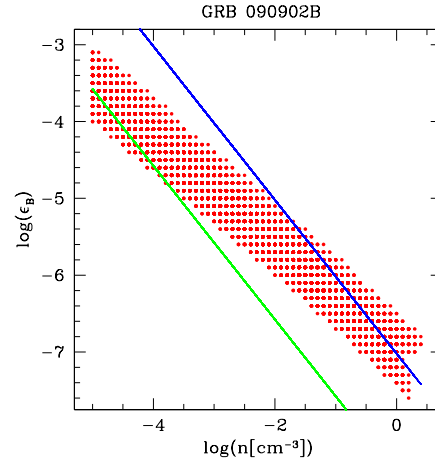


Figure 1. We determine the sub-space of the 4-D parameter space (for the forward external forward shock model with $s = 0$) allowed by the high energy data for GRB 090902B at $t=50\text{s}$ as described in §3.1. The projection of the allowed subspace onto the ϵ_B - n plane is shown in this figure (dots); the discrete points reflect the numerical resolution of our calculation. We also plot the expected ϵ_B for a shock compressed CSM magnetic field of 5 and 30 $\mu\text{-Gauss}$ as the green and blue lines respectively; for a CSM field of strength B_0 , the value of ϵ_B downstream of the shock-front resulting from the shock compressed CSM field is $\approx B_0^2 / (2\pi n m_p c^2)$, where $n m_p$ is the CSM mass density, and c is the speed of light. Note that no magnetic field amplification is needed, other than shock compression of a CSM magnetic field of $\sim 30\mu\text{G}$, to produce the $>100\text{MeV}$ photons. The synchrotron injection and cooling frequencies at $t = 50\text{s}$ are $100\text{eV} \lesssim \nu_i \lesssim 3\text{keV}$ and $30\text{MeV} \lesssim \nu_c \lesssim 100\text{MeV}$ respectively, the Lorentz factor of the blast wave at $t = 50\text{s}$ lies between 330 and 1500, and $10^{55}\text{erg} \lesssim E \lesssim 3 \times 10^{55}\text{erg}$. Note that at 0.5 day ν_i would be below the optical band, and $\nu_c > 1\text{MeV}$, and these values are consistent with the X-ray spectrum and the X-ray and optical decay indices at this time.

time, high-energy, data to late time, low-energy, flux prediction was carried out for a CSM with $s = 0$. We have also carried out the same calculation but by assuming a wind medium ($s = 2$), and in this case we find that the expected flux at late times is smaller than the observed values by a factor of 20 or more; this conclusion is drawn by comparing the late optical and X-ray fluxes predicted at a single time with the observations at that same time, i.e. without making use of the temporal decay indices observed in these bands. We pointed out above that the late time afterglow data for this burst are consistent with a uniform density medium, but not with a $s = 2$ medium. Thus, there is a good agreement between the late time afterglow data and the early $>10^2\text{MeV}$ data in regards to the property of the CSM; the two methods explore the CSM density at different radii.

3.1.2 Reverse direction

We carry out the above mentioned exercise in the reverse direction as well, i.e. we determine the ES parameter space using only the late time X-ray, optical and radio data, and use these parameters to determine the flux at 10^2MeV at early times when *Fermi*/LAT observations were made. The constraints on ES model parameters at late times are the following: (i) The X-ray and optical flux at 12.5 hr and 7.5×10^4 s, respectively, should match the ES flux at these bands and at these times, (ii) the radio flux at 1.3 d should be

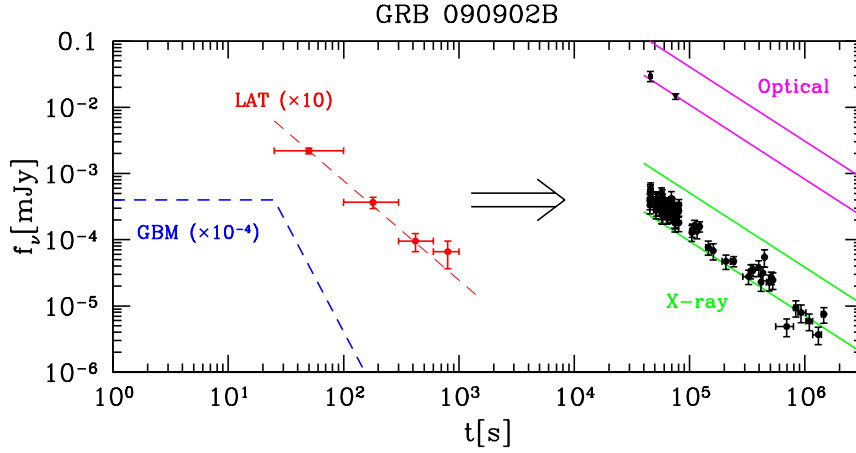


Figure 2. The optical and X-ray fluxes of GRB 090902B predicted at late times using only the high energy data at 50s (assuming synchrotron emission from external forward shock) are shown in the right half of this figure, and the predicted flux values are compared with the observed data (discrete points with error bars). The width of the region between the green (magenta) lines indicates the uncertainty in the theoretically predicted X-ray (optical) fluxes (the width is set by the error in the measurement of 100 MeV flux at 50s, and the error in the calculation of external forward shock flux due to approximations made – both these contribute roughly equally to the uncertainty in the predicted flux at late times). LAT (X-ray) data red (black) circles, are from Abdo et al. 2009c (Evans et al. 2007, 2009) and were converted to flux density at 100 MeV (1keV) using the average spectral index provided in the text. Optical fluxes are from Swenson et al. 2009 (square) and Guidorzi et al. 2009 (triangle) and were converted to flux density using $16.4\text{mag} \approx 1\text{mJy}$. The blue dashed line shows schematically the light curve observed by *Fermi*/GBM. The predicted value for the radio flux at one day has a very large range (not shown), but consistent with the observed value.

consistent with the observed value. We first show some analytical estimates and then turn to more detailed numerical calculations.

Constraint (i) is simply equation (8) set equal to the observed value of $0.4\mu\text{Jy}$ at 12.5 hr. For the analytical estimates presented here, it is not necessary to use the optical flux at late times, since both the optical and X-ray bands lie between ν_i and ν_c , so they provide identical constraints. Constraint (ii), assuming that the radio frequency is below ν_i , gives

$$f_{4.8\text{GHz}} \sim 19\text{mJy} E_{55}^{5/6} n^{1/2} \epsilon_{B,-2}^{1/3} \epsilon_{e,-1}^{-2/3} = 111\mu\text{Jy}. \quad (12)$$

Solving for ϵ_e in the last equation and substituting in constraint (i) gives an equation for ϵ_B , which is

$$\epsilon_B = \frac{6 \times 10^{-8}}{n E_{55}^2}. \quad (13)$$

This estimate is consistent with the numerical result presented on Fig. 3. Moreover, one can see that we find $\epsilon_B \propto n^{-1}$, which is exactly what is found numerically (and agrees very well with the shock-compressed CSM field prediction).

We can now predict the high-energy flux at 100 MeV and early time using the ES parameters determined using late time afterglow data in X-ray and radio bands. We use (1) at $t = 50$ s, substituting ϵ_e from (12) and n from (13), and find that the flux should be

$$f_{100\text{MeV}} \sim 200\text{nJy} E_{55}^{3/4} \epsilon_{B,-5}^{-1/4}, \quad (14)$$

in agreement with the observed value at $t = 50$ s. We now turn to our numerical results.

Using the same set of constraints presented at the beginning of this subsection, we perform our numerical calculations to determine the ES parameter space allowed by the late time ($t \gtrsim 0.5$ d) X-ray, optical and radio data and use that information to “predict” the 100 MeV flux at early times ($t \lesssim 10^3$ s). The numerical results of this exercise, for a $s = 0$ CSM medium, are also in good

agreement with the *Fermi*/LAT data as shown in Figure 4. Moreover, the flux from the ES at $t = 50$ s and 100 keV is found to be much smaller than the flux observed by *Fermi*/GBM (Fig. 4 - left panel), which is very reassuring, because otherwise this would be in serious conflict with the steep decline of the light curve observed in the sub-MeV band; this also shows that the sub-MeV and GeV radiations are produced by two different sources.

We note that the range of values for ϵ_B allowed by the late time radio, optical & X-ray afterglow data is entirely consistent with shock compressed circum-stellar medium magnetic field of strength $< 30\mu\text{G}$ (see fig. 3). We also point out that the afterglow flux depends on the magnetic field B , and $B^2 \propto \epsilon_B n$, therefore, there is a degeneracy between ϵ_B and n and that makes it very difficult to determine n uniquely.

3.2 GRB 090510

The *Fermi*/LAT and GBM observations of this burst are described in Abdo et al. (2009b) and De Pasquale et al. (2010). This short burst has very early X-ray and optical data starting only 100s after the burst. The X-ray spectrum is $\beta_x = 0.57 \pm 0.08$ (Grupe & Hoverstein 2009). The temporal decay index is $\alpha_{x,1} = 0.74 \pm 0.03$ during the initial $\sim 10^3$ s and subsequently the decay steepens to $\alpha_{x,2} = 2.18 \pm 0.10$ with a break at $t_x = 1.43^{+0.09}_{-0.15}$ ks. The optical data shows $\alpha_{opt,1} = -0.5^{+0.11}_{-0.13}$ and $\alpha_{opt,2} = 1.13^{+0.11}_{-0.10}$ with a break at $t_{opt} = 1.58^{+0.46}_{-0.37}$ ks (De Pasquale et al. 2010).

In the context of the ES model (also considered by Gao et al. 2009, Ghirlanda, Ghisellini, Nava 2010 and De Pasquale et al. 2010 for the case of this specific burst), the data suggests that $\nu_x < \nu_c$, because in this case $\beta_x = (p-1)/2$, so $p = 2.14 \pm 0.16$ and the temporal decay index (for $s = 0$) is $\alpha_x = 3(p-1)/4 = 0.86 \pm 0.12$ consistent with the observed value of $\alpha_{x,1}$. If we take $\nu_x > \nu_c$, then $\beta_x = p/2$, so $p = 1.14 \pm 0.16$ and the temporal

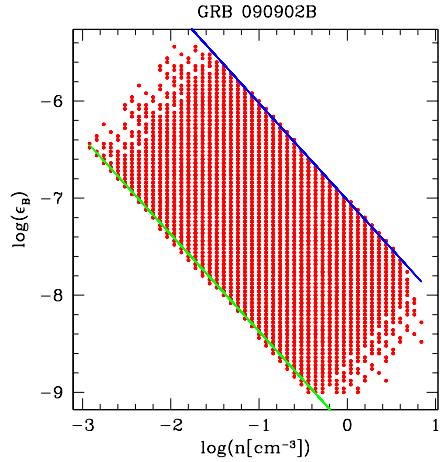


Figure 3. We determine the sub-space of the 4-D parameter space (for the external forward shock model with $s = 0$) allowed by the late time ($t > 0.5$ day) X-ray, optical and radio data for GRB 090902B as described in §3.1. The projection of the allowed subspace onto the ϵ_B - n plane at $t = 0.5$ day is shown in this figure (dots). We also plot the expected ϵ_B for a shock compressed CSM magnetic field of 2 and 30 μ -Gauss as the green and blue lines, respectively; for a CSM field of strength B_0 , the value of ϵ_B downstream of the shock-front resulting from the shock compressed CSM field is $\approx B_0^2/(2\pi nm_p c^2)$, where nm_p is the CSM mass density, and c is the speed of light. Note that no magnetic field amplification is needed, other than shock compression of a CSM magnetic field of strength $\lesssim 30 \mu$ G, to produce the late time X-ray, optical and radio data. We arrived at this same conclusion from the modeling of early time > 100 MeV radiation alone (see fig. 1).

decay index should have been $\alpha_x = (3p + 10)/16 = 0.84 \pm 0.03$, since $p < 2$, which is consistent with the observed temporal decay, however, the expected optical light curve index for this value of p is $\alpha_{opt} = -(p + 2)/(8p - 8) = -2.8$, which is inconsistent with the observed value of $\alpha_{opt,1}$ (see next paragraph). The X-ray afterglow data also shows that the medium in the vicinity of the burst must have been of constant density. This is because, for an $s = 2$ medium, the expected temporal decay of the X-ray flux, when $\nu_x < \nu_c$, is $\propto t^{-(3p-1)/4} = t^{-1.36}$ – much steeper than the observed decline of $t^{-0.74}$ – while for $s = 0$ the expected decline is consistent with observations (Gao et al. 2009).

Given the fact that the break in the optical light curve and that in the X-ray light curve occur at the same time, i.e. $t_x = t_{opt}$, it is unlikely that the emission in these two bands comes from two different, unrelated sources. Thus, it is natural to attribute both the optical and X-ray emissions to the external forward shock. The fact that the optical light curve is rising during the first ~ 0.5 hr as $t^{1/2}$ means that $\nu_{opt} < \nu_i$ during this time period (Panaitescu & Kumar 2000), where ν_{opt} is the optical band. The break seen in both light curves can be attributed to the jet break. The X-ray light curve decay of $t^{-2.2}$ for $t > 1.4 \times 10^3$ s agrees very well with the expected post-jet-break light curve of $\propto t^{-p} = t^{-2.12 \pm 0.14}$ (Rhoads 1999), and suggests a jet opening angle of $\sim 1^\circ$ (Sari, Piran & Halpern, 1999). The reason that $\alpha_{opt,2}$ is not as steep can be understood the following way. At the time of the jet break, the optical band is below ν_i , therefore, the light curve decays as $\propto t^{-1/3}$ instead of $\propto t^{-p}$ (Rhoads 1999). At later times, when ν_i , which is decreasing rapidly, crosses the optical band, the optical light curve will transition slowly from $\propto t^{-1/3}$ to $\propto t^{-p}$, and that is why $\alpha_{opt,2}$ is not as large as $\alpha_{x,2}$; the timescale for this transition can be long/short depending on how far above γ_i the asymptotic distri-

bution of $n(\gamma) \propto \gamma^{-p}$ is attained. This interpretation is supported by the results of our numerical calculation shown in Figure 5 — we obtain a value of $\nu_i \sim 500$ eV at 100s, which should cross the optical band at ~ 4000 s – a factor of ~ 3 larger than the observed time of the jet break. This idea can be tested with optical data available at much later times: it should show the light curve slowly steepening to the asymptotic value of $\propto t^{-p}$. Moreover, the optical spectrum before the break in the light curve ($t < t_{opt}$) should be consistent with $\nu^{1/3}$.

Is it possible that the rise of the optical band light curve might be due to the onset of the ES, while the initial X-ray emission (until the break at ~ 1.4 ks) and the gamma-ray photons are from the “internal shock” mechanism (De Pasquale et al. 2010)? This seems unlikely, given that the density of the CSM required for the deceleration time of the GRB jet to be $\sim 10^3$ s (t_{opt}) is extremely low, as can be seen from the following equation

$$n = \frac{3E(1+z)^3}{32\pi c^5 m_p \Gamma^8 t_{peak}^3}, \quad (15)$$

where m_p is the mass of the proton, c is the speed of light, Γ is the initial Lorentz factor of the GRB jet, t_{peak} is the time when the peak of the light curve is observed and E is the isotropic energy in the ES. For GRB 090510, Γ was determined to be $\Gamma \gtrsim 10^3$ by using $\gamma\gamma$ opacity arguments (Abdo et al. 2009b), which is a limit applicable to the scenario proposed by De Pasquale et al. (2010), where MeV and GeV photons are produced in the same source. We take $t_{peak} \sim 10^3$ s and $E \sim E_{\gamma,iso}$ and find that we need a CSM density of $n \approx 10^{-9} E_{53} \Gamma_3^{-8} t_{peak,3}^{-3} \text{cm}^{-3}$, which is much smaller than the mean density of the Universe at this redshift, and therefore unphysical. Even though there is a strong dependence of CSM density on Γ , the upper limit on density provided above cannot be increased by more than a factor of ~ 10 , since the error in the determination of Γ is much less than a factor of 2 (Abdo et al. 2009b). Thus, the possibility that the peak of the optical light curve at $\sim 10^3$ s is due to the deceleration of the GRB jet seems very unlikely. We note that in the scenario we present in this paper, the > 100 MeV emission observed by *Fermi*/LAT and the lower energy ($\lesssim 1$ MeV) observed by *Fermi*/GBM are produced by two different sources, therefore, the pair-production argument can’t be used to constrain Γ . However, in this scenario, the deceleration time for the GRB jet is $\lesssim 1$ s, and that means that the peak of the optical light curve at $\sim 10^3$ s cannot correspond to the deceleration time.

We conclude that the available data suggest that optical and X-ray photons are coming from the same source (ES model). We now consider whether the observed > 100 MeV emission is also consistent with the ES model. We first use the observed data to show that > 100 MeV, X-ray and optical data are produced by the ES, then we provide some analytical estimates of the ES model parameters and later show the results of our detailed numerical results in the figures.

AGILE/GRID reported a photon count in the 30 MeV–30 GeV band of $1.5 \times 10^{-3} \text{cm}^{-2} \text{s}^{-1}$ at 10s, and the light curve was reported to decline as $t^{-1.3 \pm 0.15}$ (Giuliani et al. 2010). Therefore, the photon flux at 100s in this band is estimated to be $\sim 7.5 \times 10^{-5} \text{cm}^{-2} \text{s}^{-1}$ (Ghirlanda, Ghisellini, Nava, 2010; have also reported a single power-law decline of flux in the *Fermi* LAT band from ~ 1 s to 200s). The Swift/XRT reported a photon flux of $0.07 \text{cm}^{-2} \text{s}^{-1}$ in the 0.3–10 keV band at 100s. Using the spectrum reported in the Swift/XRT band (Grupe & Hoverstein 2009) — which is entirely consistent with the spectrum found in the AGILE/GRID band (Giuliani et al. 2010) — to extrapolate the observed photon count in the XRT band to the GRID band we find the expected photon flux at

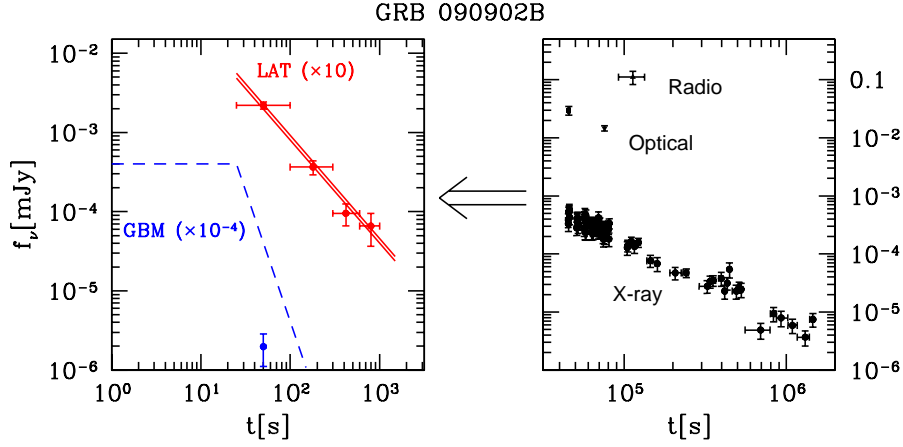


Figure 4. Using the X-ray, optical and radio data of GRB 090902B at late times (right panel) we constrain the external forward shock parameters, and then use these parameters to predict the 100 MeV flux at early times (left panel). The region between the red lines shows the range for the predicted flux at 100 MeV; note the remarkably narrow range for the predicted 100 MeV flux in spite of the large spread to the allowed ES parameters as shown in fig. 3. The blue point (left panel) indicates the flux at 100keV and 50s that we expect from the ES model; note that the ES flux at 100 keV falls well below the observed *Fermi*/GBM flux shown schematically by the dashed line in the left panel, and that is why the GBM light curve undergoes a rapid decline with time ($\sim t^{-3}$) at the end of the prompt burst phase. The radio flux is taken from van der Host et al. 2009. All other data are the same as in Figure 2.

100s in the 30 MeV–30 GeV band of $7.9 \times 10^{-5} \text{ cm}^{-2} \text{ s}^{-1}$, and that is consistent with the flux observed by AGILE.

The peak of the optical light curve was observed at ~ 1000 s with a value of $\sim 100 \mu\text{Jy}$, and the X-ray flux at 1000 s and $\sim 4\text{keV}$ was $2.2 \mu\text{Jy}$ (De Pasquale et al. 2010). Since we attribute the optical light curve peak with the crossing of ν_i through the optical band, then the peak of the optical light curve determines the synchrotron flux at the peak of the spectrum. Therefore, using the X-ray flux at 1000 s and the X-ray spectrum we can extrapolate back to optical band (2 eV) and we find a flux of $170 \mu\text{Jy}$, which is consistent, within a factor of better than 2, with the observed optical value at this time. Therefore, we can conclude that >100 MeV, X-ray and optical emissions are all produced by the same source, and that source must be the external forward shock as that is known to produce long lasting radiation in the X-ray and optical bands with a well known closure relation between α and β that is observed in GRB 090510 in all energy bands.

Using the data in the LAT, XRT and optical bands we can determine the ES parameters for GRB 090510. The following observational constraints must be satisfied by the allowed ES parameters: (i) The flux at 100 MeV and 100s should be equal to the observed value (Table 2), (ii) $\nu_c < 100$ MeV at 100s, (iii) the X-ray flux at 1000s and $\sim 4\text{keV}$ should be equal to the observed value of $2.2 \mu\text{Jy}$ (De Pasquale et al. 2010), and (iv) the flux at the peak of synchrotron spectrum should be $\sim 100 \mu\text{Jy}$ (De Pasquale et al. 2010). This last constraint arises because the optical flux peaks when ν_i passes the optical band, and therefore the peak synchrotron flux should be equal to the measured peak optical flux; it should be noted that the peak synchrotron flux for $s = 0$ according to the ES model does not change with time as long as the shock front moves at a relativistic speed.

We present some analytical estimates for the ES parameters before showing our detailed numerical results. The ES flux at 100 MeV and $t = 100$ s, assuming that 100 MeV is above ν_c is given by (1) and is

$$f_{100\text{MeV}} \sim 2.4 \times 10^{-6} \text{ mJy } E_{53}^{1.1} \epsilon_{B,-2}^{0.1} \epsilon_{e,-1}^{1.4} = 14 \text{ nJy}, \quad (16)$$

which is the constraint (i). The flux at 4 keV and 1000s, assuming that it is between ν_i and ν_c is given by

$$f_{4\text{keV}} \sim 3 \text{ mJy } E_{53}^{1.35} n^{0.5} \epsilon_{B,-2}^{0.85} \epsilon_{e,-1}^{1.4} = 2.2 \mu\text{Jy}, \quad (17)$$

which is constraint (iii). And lastly, constraint (iv) is that the peak synchrotron flux should equal the flux at the peak of the optical light curve, i.e.,

$$f_p \sim 12 \text{ mJy } E_{53} n^{1/2} \epsilon_{B,-2}^{1/2} = 100 \mu\text{Jy}. \quad (18)$$

Just as was done for GRB090902B, constraint (ii) gives a lower limit on ϵ_B , which in the case for this GRB is not too useful. Instead, we can solve ϵ_e from (16) and substitute it in (17), which gives

$$\epsilon_B = \frac{1 \times 10^{-6}}{E_{53}^{1/3} n^{2/3} (1+Y)^{4/3}}, \quad (19)$$

consistent with the numerical calculation presented in Fig. 5. Also, with this last expression and using (18) we find that the CSM density for this GRB is

$$n \sim 0.3 \text{ cm}^{-3} (1+Y)^4 E_{53}^{-5}, \quad (20)$$

which is also consistent with the fact that we only find numerical solutions with CSM densities lower than $\sim 0.1 \text{ cm}^{-3}$.

For the ES parameters of this burst, the cooling frequency at 100 s can be estimated to be

$$\nu_c \sim 76 \text{ eV } E_{53}^{-1/2} n^{-1} \epsilon_{B,-2}^{-3/2} (1+Y)^{-2}, \quad (21)$$

and substituting n from (18) gives $\nu_c \sim 1 \text{ MeV } E_{53}^{3/2} \epsilon_{B,-2}^{-1/2} (1+Y)^{-2}$. Thus, for $\epsilon_B \sim 10^{-5}$ we find $\nu_c \sim 30 \text{ MeV}$. The injection frequency at 100 s is given by

$$\nu_i \sim 240 \text{ eV } E_{53}^{1/2} \epsilon_{B,-2}^{1/2} \epsilon_{e,-1}^2, \quad (22)$$

and substituting ϵ_e from (16) one finds $\nu_i \sim 250 \text{ eV } E_{53}^{-1.07} \epsilon_{B,-5}^{0.36}$. These values of ν_i and ν_c are consistent with the values obtained

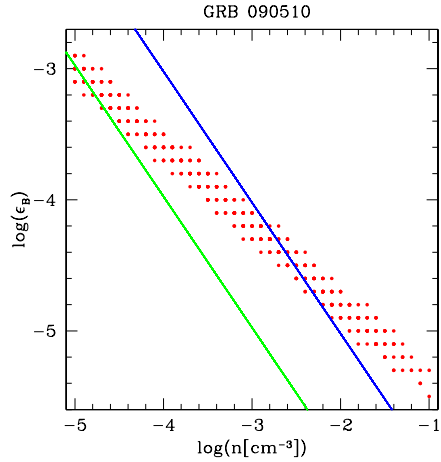


Figure 5. Using the observational constraints mentioned in the text (§3.2), we determine the sub-space of 4-D parameter space (for the external forward shock with $s = 0$) allowed by the data for GRB 090510 at $t = 50$ s. We show the projection of the allowed subspace onto the ϵ_B - n plane in this figure (dots); the region agrees with the expected ϵ_B from shock-compressed CSM magnetic field of $\lesssim 30\mu\text{G}$ (the green and blue lines show $10\mu\text{G}$ and $30\mu\text{G}$, respectively). The other parameters for the ES solution at this time are: The Lorentz factor of the blast wave is between 260 and 970, $0.1 < \epsilon_e < 0.7$ and $10^{53}\text{erg} \lesssim E \lesssim 4 \times 10^{53}\text{erg}$. At $t = 100$ s, we also find $Y < 4$, $\nu_i \sim 500$ eV, $\nu_c \sim 40$ MeV.

with detail numerical calculations and reported in the Fig. 5 caption.

The detailed numerical results of the parameter search can be found in Figure 5; the sub-space of the 4-D parameter space allowed by the data for GRB 090510 is projected on the 2-D ϵ_B - n plane, which is a very convenient way of looking at the allowed sub-space. Note that all the available data for GRB 090510 can be fitted by the ES model and that the value of n allowed by the data is less than 0.1 cm^{-3} , which is in keeping with the low density expected in the neighborhood of short bursts. Moreover, ϵ_B for the entire allowed part of the 4-D sub-space is small, and its magnitude is consistent with what one would expect for the CSM magnetic field of strength $\lesssim 30\mu\text{G}$ that is shock compressed by the blast wave (Fig. 5). The ES shock model provides a consistent fit to the data from optical to $>10^2\text{MeV}$ bands as can be clearly seen in Figure 6. The ES parameters found for this GRB can be found in the Fig. 5 caption.

3.3 GRB 080916C

The *Fermi*/LAT and GBM observations for this burst have been presented in Abdo et al. (2009a). For this burst, the optical and X-ray observations started about 1d after the burst and both bands are consistent with $f_\nu(t) \propto \nu^{-0.5 \pm 0.3} t^{-1.3 \pm 0.1}$ (Greiner et al. 2009).

The fact that the optical light curve is decaying as $t^{-1.3}$ means that ν_i is below the optical band at 1 day, because if ν_i is above the optical band, then the light curve should be rising as $\propto t^{1/2}$ (as in the case of GRB090510). Moreover, the shallow spectral index in the Swift/XRT band ($\beta_x < 1$) suggests that $\nu_c > 10\text{keV}$ at 1 day. The X-ray and optical data together yield a spectral index of 0.65 ± 0.03 , and therefore $p = 2.3 \pm 0.06$ which is consistent with the *Fermi*/LAT spectrum (see Table 1). The value of p can be used to calculate the time dependence of the light curve, and that is found to be $t^{-0.98}$ ($t^{-1.48 \pm 0.05}$) for $s = 0$ ($s = 2$) CSM. Thus, $s = 2$ CSM is preferred by the late time optical and X-ray afterglow data

(Kumar & Barniol Duran 2009; Gao et al. 2009; Zou, Fan & Piran 2009).

Using the early >100 MeV data only, we determine the ES model parameters. With these parameters, we can then predict the X-ray and optical fluxes at late times, i.e. the forward direction approach. The constraints that should be satisfied are: (i) The ES flux at 100 MeV and 150 s should match the observed value (Table 2), (ii) $\nu_c < 100$ MeV to be consistent with the observed spectrum, and (iii) the ES flux at 150 s should be smaller than the observed value to allow the 100 keV flux to decay rapidly as observed. These constraints are the same as the ones presented for the case of GRB090902B and the analytical approach is the same as the one presented on §3.1, therefore, we omit the details here. The ES parameters obtained numerically can be found in fig. 2 of Kumar & Barniol Duran (2009). With these parameters the X-ray and optical flux at late times can be calculated, and we find these in excellent agreement with the observations (Figure 7).

It is important to note here that this extrapolation from high-energy early time data to low energy, late time, flux prediction was carried out for a circum-stellar medium with $s \sim 2$. We have also carried out the same calculation but for a uniform density medium ($s = 0$), and in this case the theoretically calculated flux at late times is larger than the observed values by a factor of ~ 5 or more; the factor of 5 discrepancy is much larger than error in the flux calculation. We pointed out above that the late time afterglow data for this burst are consistent with a $s = 2$ medium but not $s = 0$ medium. Thus, there is a nice agreement between the late time afterglow data and the early $>10^2\text{MeV}$ data — which explore very different radii — in regards to the density stratification of the CSM.

We have carried out the exercise in the “reverse direction” as well. Using only the late X-ray and optical data, we determine the ES parameters. The observational constraints that need to be satisfied are: (i) The ES flux at X-ray and optical energies at 1 d should match the observed values, (ii) we should have the ordering $\nu_i < \nu_{opt} < \nu_X < \nu_c$ to be consistent with the observed spectrum, (iii) the ES flux at 150 s should be smaller than the observed value to allow the 100 keV flux to decay rapidly as observed, and (iv) the Lorentz Factor of the ejecta should be $\gtrsim 60$ at 1 d, since we don’t want Γ to be too small at the beginning of the burst, because this would contradict estimates done at early times (Greiner et al. 2009). Since the analytical approach is very similar to the one for GRB090902B, we omit it here – the only difference is that it must be done for a wind-like medium, since the data of this GRB prefers it. The ES parameters can be found numerically and with these parameters we predict the >100 MeV flux at early times. This predicted flux agrees with the *Fermi*/LAT observations as shown in fig. 3 of Kumar & Barniol Duran (2009).

4 DISCUSSION AND CONCLUSION

The *Fermi* Satellite has detected 12 GRBs with >100 MeV emission in about one year of operation. In this paper we have analyzed the >100 MeV emission of three of them: two long-GRBs (090902B and 080916C) and one short burst (GRB 090510), and find that the data for all three bursts are consistent with synchrotron emission in the external forward shock. This idea was initially proposed in our previous work on GRB 080916C (Kumar & Barniol Duran 2009), shortly after the publication of this burst’s data by Abdo et al. (2009a). Now, there are three GRBs for which high energy data has been published, and for all of them we have presented here multiple lines of evidence that >100 MeV photons, subse-

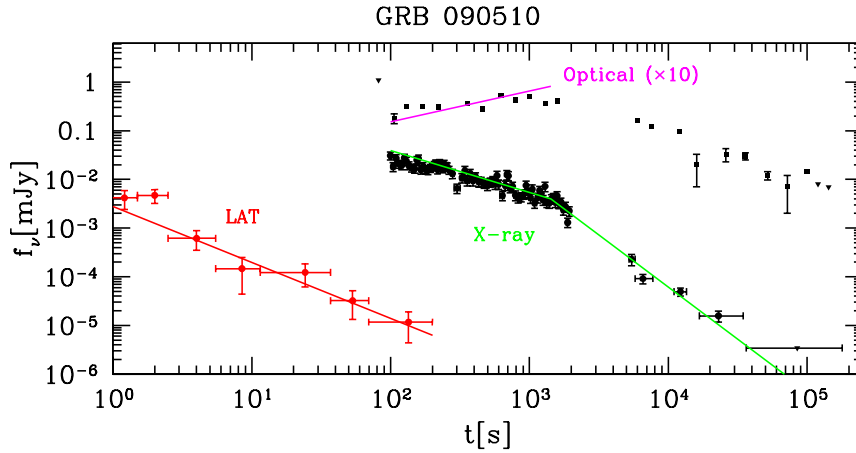


Figure 6. Shown in this figure are data for GRB 090510 obtained by *Fermi*/LAT (>100 MeV), Swift/XRT (X-ray) and Swift/UVOT (optical) data, and a fit to all these data by the external forward shock model (solid lines). The jet break seen in X-ray has been modeled with a power-law, $\propto t^{-p}$; the optical light curve after the jet break should show a shallower decay $\propto t^{-1/3}$, because at this time $\nu_{opt} < \nu_i$, but then it slowly evolves to an asymptotic decay $\propto t^{-p}$ at later times (Rhoads 1999). The LAT (X-ray) data are from De Pasquale et al. 2009 (Evans et al. 2007, 2009) and have been converted to flux density at 100 MeV (1 keV) using the average spectral index mentioned in the text (§3.2). The optical data (squares) are from De Pasquale et al. (2010). Triangles mark upper limits in the X-ray and optical light curves.

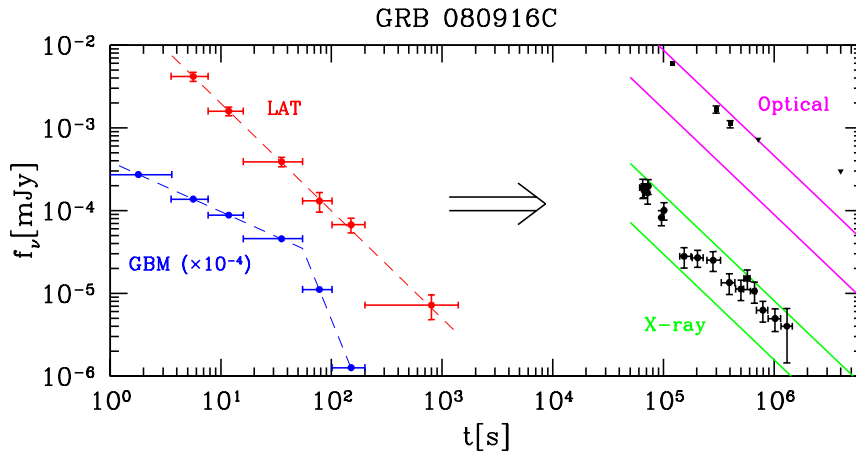


Figure 7. The optical and X-ray fluxes of GRB 080916C predicted at late times using only the high energy data at 150s (assuming synchrotron emission from external forward shock) are shown in the right half of this figure, and the predicted flux values are compared with the observed data (discrete points with error bars). The width of the region between the green (magenta) lines indicates the uncertainty in the theoretically calculated X-ray (optical) fluxes. The LAT (Abdo et al. 2009a) and X-ray fluxes (Evans et al. 2007, 2009) at 100 MeV and 1keV, respectively, have been converted to mJy the same way as done for Figure 2. Optical fluxes (squares) are from Greiner et al. 2009 (triangles are upper limits). GBM flux at 100keV – blue filled circles – is taken from Abdo et al. 2009a. The thin dashed lines connecting LAT and GBM data are only to guide the eye.

quent to the prompt GRB phase, were generated in the external forward shock. The reason that high energy photons are detected from only a small fraction of GRBs observed by *Fermi* is likely due to the fact that the high energy flux from the external forward shock has a strong dependence on the GRB jet Lorentz factor, and therefore very bright bursts with large Lorentz factors are the only ones detected by *Fermi*/LAT (this was pointed out by Kumar & Barniol Duran 2009, who also suggested that there should be no difference in long and short bursts, as far as the >100 MeV emission is concerned - the high energy flux is only a function of burst energy and time, eq. 1).

We have analyzed the data in 4 different ways, and all of them lead to the same conclusion regarding the origin of $>10^2$ MeV photons. First, we verified that the temporal decay index for the >100 MeV light curve and the spectral index are consistent with the closure relation expected for the synchrotron emission in the external forward shock. Second, we calculated the expected magnitude of the synchrotron flux at 100 MeV according to the external forward shock model and find that to be consistent with the observed value. Third, using the >100 MeV data only, we determined the external shock parameters, and from these parameters we predict the X-ray and optical fluxes at late times and find that these predicted fluxes

are consistent with the observed values within the uncertainty of our calculations, i.e. a factor of two (see figs. 2, 7). And lastly, using the late time X-ray, optical and radio fluxes — which the GRB community has believed for a long time to be produced in the external forward shock — we determine the external shock parameters, and using these parameters we predict the expected >100 MeV flux at early times and find the flux to be in agreement with the observed value (see fig. 4). The fact that the >100 MeV emission and the lower energy ($\lesssim 1$ MeV) emission are produced by two different sources at two different locations suggests that we should be cautious when using the highest observed photon energy and pair-production arguments to determine the Lorentz factor of the GRB jet.

We point out that the external shocks for these bursts were nearly adiabatic, i.e. radiative losses are small. The evidence for this comes from two different observations: (1) the late time X-ray spectrum lies in the adiabatic regime; (2) a radiative shock at early times (close to the deceleration time) would produce emission in the $10\text{--}10^2$ keV band far in excess of the observed limits. We find that radiative shock is not needed to explain the temporal decay index of the >100 MeV light curve as suggested by (Ghisellini, Ghirlanda, Nava 2010), provided that the observing band is above all synchrotron characteristic frequencies.

We find that the magnetic field required in the external forward shock for the observed high and low energy emissions for these three bursts is consistent with shock-compressed magnetic field in the CSM; the magnetic field in the CSM – before shock compression – should be on the order of a few tens of micro-Gauss (see figs. 1, 3 and 5). For these three bursts, at least, no magnetic dynamo is needed to operate behind the shock front to amplify the magnetic field.

The data for the short burst (GRB 090510) are consistent with the medium in the vicinity of the burst (within ~ 1 pc) being uniform and with density less than 0.1 cm^{-3} ; the data rules out a CSM where $n \propto R^{-2}$. On the other hand, the data for one of the two long *Fermi* bursts (GRB 080916C) prefers a wind like medium and the other (GRB 090902B) a uniform density medium; these conclusions are reached independently from late time afterglow data alone and from the early time high energy data projected to late time using the 4-D parameter space technique described in §3.

It is also interesting to note that the power-law index of the energy distribution of injected electrons (p) in the shocked fluid, for all the three *Fermi* bursts analyzed in this work, is 2.4 to within the error of measurement, suggesting an agreement with the *Fermi* acceleration of particles in highly relativistic shocks, e.g. Achterberg et al. (2001); a unique power-law index for electrons' distribution in highly relativistic shocks is not found in all simulations. The study of high energy emission close to the deceleration time of GRB jets is likely to shed light on the onset of collisionless shocks and particle acceleration process.

It might seem surprising that we are able to fit all data (optical, X-ray, $\lesssim 10^2$ MeV) for these three *Fermi* bursts with just a few parameters for the external forward shock. This is in sharp contrast to Swift bursts which often display a variety of puzzling (poorly understood) features in their afterglow light curves. There are two reasons that these *Fermi* bursts can be understood using a very simple model (external forward shock). (1) The data for the two long *Fermi* bursts (080916C and 090902B) are not available during the first 1/2 day, and that is precisely the time frame when complicated features (plateau, etc., eg. Nousek et al. 2006, O'Brien et al. 2006) are seen in the X-ray afterglow light curves of Swift bursts (we note that the external forward shock model in its sim-

plest form can't explain these features) — however, the afterglow data at later times is almost invariably a smooth single (or double) power-law function that can be modeled by synchrotron emission from an external forward shock. (2) For very energetic GRBs — the three bursts we have analyzed in this paper are among the brightest bursts in their class — the progenitor star is likely to be completely destroyed leaving behind very little material to fall back onto the compact remnant at the center to fuel continued activity and give rise to complex features during the first few hours of the X-ray afterglow light curve (Kumar, Narayan & Johnson, 2008). To summarize, the GRB afterglow physics was simple in the decade preceding the launch of Swift, and then things became quite complicated, and now the *Fermi* data might be helping to clear the fog and reveal the underlying simplicity once again.

ACKNOWLEDGMENTS

RBD thanks Massimiliano De Pasquale for clarifying some aspects of the data of GRB 090510. We also thank Alex Kann for useful discussions about the optical data. We thank the referee for a constructive report. This work has been funded in part by NSF grant ast-0909110. This work made use of data supplied by the UK Swift Science Data Centre at the University of Leicester.

REFERENCES

- Abdo A. et al., 2009a, *Science*, 323, 1688
 Abdo A. et al., 2009b, preprint (arXiv:0908.1832)
 Abdo A. et al., 2009c, *ApJL*, 706, 138
 Achterberg, A., Gallant, Y.A., Kirk, J.G., and Guthmann, A.W., 2001, *MNRAS* 328, 393
 Blandford R. D., McKee C. F., 1976, *Phys. Fluids*, 19, 1130
 De Pasquale M. et al. 2010, *ApJ*, 709, 146
 Evans P.A. et al., 2007, *A&A*, 469, 379
 Evans P.A. et al., 2009, *MNRAS*, 397, 1177
 Fan Y.Z., Piran T., 2008, *Front. Phys. China*, 3, 306
 Gao W.-H., Mao J., Xu D., Fan Y.Z., 2009, *ApJ*, 706, L33
 Gehrels N., Ramirez-Ruiz E., Fox D.B., 2009, *ARA&A*, 47, 567
 Ghirlanda G., Ghisellini G., Nava L., 2010, *A&A*, 510, 7
 Ghisellini G., Ghirlanda G., Nava L., 2010, *MNRAS*, 403, 926
 Giuliani A. et al., 2010, *ApJ*, 708, L84
 Greiner J. et al., 2009, *A&A*, 498, 89
 Grupe D., Hoverstein E., 2009, *GCN Circ.*, 9341
 Guidorzi C. et al., 2009, *GCN Circ.*, 9875
 Gupta N, Zhang B., 2007, *MNRAS*, 380, 78
 Kumar P., 2000, *ApJ*, 538, 125
 Kumar P., Barniol Duran R., 2009, *MNRAS*, 400, L75
 Kumar P., McMahon E., 2008, *MNRAS*, 384, 33
 Kumar P., Narayan R., 2009, *MNRAS*, 395, 472
 Kumar P., Narayan R., Johnson J.L., 2008, *MNRAS*, 388, 1729
 Mészáros P., 2006, *Rep. Prog. Phys.*, 69, 2259
 Mészáros P., Rees M.J., 1993, *ApJ*, 405, 278
 Nousek J.A. et al., 2006, *ApJ*, 642, 389
 O'Brien P. et al. 2006, *ApJ*, 647, 1213
 Omodei N. et al., 2009, *Proceedings for 31st Int'l Cosmic-Ray Conference*, preprint (arXiv:0907.0715)
 Paczyński B., Rhoads J.E., 1993, *ApJ*, 418, L5
 Panaitescu A., Kumar P., 2000, *ApJ*, 543, 66
 Panaitescu A., Kumar P., 2001, *ApJ*, 560, L49
 Panaitescu A., Kumar P., 2002, *ApJ*, 571, 779
 Pandey S.B., Zheng W., Yuan F., Akerlof C., 2009, *GCN Circ.*, 9878
 Pandey S.B. et al., 2010, *ApJ*, 714, 799
 Piran T., 2004, *Rev. Modern Phys.*, 76, 1143
 Rees M.J., Mészáros P., 1992, *MNRAS*, 258, 41P

- Rhoads J.E., 1999, *ApJ*, 525, 737
Rybicki G. B., Lightman A. P., 1979, *Radiative Processes in Astrophysics*.
Wiley-Interscience Press, New York
Sari R., Piran T., Narayan R., 1998, *ApJ*, 497, L17
Sari R., Piran T., Halpern, J.P., 1999, *ApJ*, 519, L17
Swenson C., Stratta G., 2009, *GCN Circ.*, 9877
van der Horst A.J., Kamble A.P., Wijers R.A.M., Kouveliotou C., 2009,
GCN Circ., 9883
Woosley S.E., Bloom J.S., 2006, *ARA&A*, 44, 507
Zhang B., 2007, *Chinese J. Astron. Astrophys.*, 7, 1
Zhang B., Mészáros P., 2004, *Int. J. Modern Phys. A*, 19, 2385
Zou Y.C., Fan Y.Z., Piran T., 2009, *MNRAS*, 396, 1163